PHYSICAL REVIEW A VOLUME 43, NUMBER 6 15 MARCH 1991

Photoabsorption in hot plasmas based on the ion-sphere and ion-correlation models

Balazs F. Rozsnyai
Lawrence Livermore National Laboratory, P. O. Box 808, L-299, Livermore, California 94550

(Received 20 August 1990)

In hot plasmas the theoretically predicted photoabsorption cross sections rest upon the electronic states predicted by the plasma model. We compare the theoretical photoabsorption based on two models, the ion-sphere model and the ion-correlation model. We discuss the underlying physics and present calculations for iron, aluminum, and bromine plasmas, and also for a mixture of 14 elements under conditions occurring below the convective region of the sun.

I. INTRODUCTION

Photoabsorption is a key element for understanding radiative properties of laboratory and astrophysical plasmas. For this reason it has been at the center of interest for a long time. In fact, the early attempts to compute opacities in stellar interiors were made in the days of the old quantum theory.[1] In subsequent years with the appearance of wave mechanics, the theoretical basis for opacity calculations was greatly enhanced, and numerous papers have appeared in the literature covering this subject. The first works were done within the framework of the hydrogenic approximation,[2] where simple hydrogenic formulas were used for the calculation of oscillator strengths and electron energies. In subsequent works, as the temperature-density-dependent Thomas-Fermi theory was developed,[3,4] the Thomas-Fermi shell model formed the quantum-mechanical basis of opacity calculations.[5] The author of this report applied first a temperature- and density-dependent Hartree-Slater self-consistent model[6] for opacity calculations. With the growing interest in the physics of hot plasmas, a number of papers appeared treating the equation of state in the density-functional approach.[7–10] In all the above references the underlying equation of state was based on the "average-atom" (AA) concept, which assumes that the electronic levels (bound and free) are populated according to the Fermi statistics. Also, in all the above references the quantum mechanics was treated within the framework of the central-field approximation, which we retain in this paper with the understanding of the limitations it imposes on all models. With regard to boundary conditions, and to the question as to how a central ion interacts with the plasma, the presently used models can be placed into two categories. The ion-sphere (IS) model assumes that each representative ion is enclosed in a spherical volume whose radius, the ion-sphere radius, is determined by the density of the plasma, and all Z electrons, bound and free, are confined within the ion sphere, therefore charge neutrality within the ion sphere is assured. In the ion-correlation (IC) model, the plasma is represented by an infinite polarizable medium into which each ion is immersed. In the IC model, charge neutrality requires that far away from the center of the nucleus the positive and negative charges cancel each other out to form a neutral background, and all equations are subject to this boundary condition. In the high-temperature limit, the IC model becomes the standard Debye-Hückel model. Reference 6 is an example for the AA-IS model, whereas Refs. 7–10 are in the framework of the AA-IC model. Although Refs. 7–9 are quite detailed in the treatment of the electronic structure of the plasma, the subject of photoabsorption is covered only in a rudimentary fashion in Ref. 9, and in a somewhat more detailed fashion in Ref. 10. The author is not aware of a comprehensive comparison of the total photoabsorption predicted by the IS and IC models, and this is the purpose of this paper. A comparison between the free-free Gaunt factors consistent with the boundary conditions of the two models was presented in a recent paper by Rozsnyai and Lamoureux;[11] here we concentrate on the total photoabsorption, which includes free-free absorption (inverse bremsstrahlung), photoionization, and line absorption. In Sec. II we present the theoretical basis of the AA-IS and AA-IC models, and in Sec. III we present computational results.

II. THEORY

A complete set of the self-consistent equations for the AA-IS model was given in Ref. 6. Here we recapitulate the basic equations as applicable for the AA-IS and AA-IC models. For the bound and continuum states we use a one-particle equation which is justifiable from density-functional theory,

$$H\Psi_{nljm}=\varepsilon_{nlj}\Psi_{nljm}\ , \tag{2.1}$$

where H is a one-particle Schrödinger or Dirac Hamiltonian containing the self-consistent electron potential. The latter has contributions from several sources and can be written as

$$V(r)=-Z/r+V_e(r)+V_{\rm xc}(r)+V_+(r)\ , \tag{2.2}$$

where r stands for the distance from the center of the nucleus and Z for the nuclear charge. From here on, unless stated otherwise, all quantities are given in atomic units (a.u.). In Eq. (2.2), V_e is the contribution resulting from the classical electron-electron interaction, $V_{\rm xc}$ is a local exchange-correlation potential, and V_+ is a contribution to the potential from the distribution of the positive ions in the vicinity of the central radiating ion. The classical electron-electron potential is determined from Poisson's equation

$$\nabla^2 V_e(r) = -4\pi\rho_e(r) , \tag{2.3}$$

where $\rho_e(r)$ stands for the electron density. The latter is given by

$$\rho_e(r) = \sum_n p_n |\Psi(r)|^2 , \tag{2.4}$$

where the summation goes over all the bound and free states, and p_n stands for the occupancy of the level n. The cardinal assumption of the AA model is that under the conditions of local thermodynamic equilibrium (LTE), the occupancies are given by the Fermi statistics

$$p_n = g_n \{\exp[(\varepsilon_n - \mu)/kT] + 1\}^{-1} , \tag{2.5}$$

where g_n and ε_n stand for the statistical weight and energy of the level n, and kT and μ stand for the temperature and Fermi level, all in energy units. In the algorithms used in this paper the electron density given by Eq. (2.4) is divided into bound and free densities as

$$\rho_e(r) = \sum_{n=1}^{b} p_n |\Psi_n(r)|^2 + \frac{4\pi}{h^3}(2mkT)^{3/2} I_{1/2}\left[\frac{\mu - V(r)}{kT}\right] , \tag{2.6}$$

where the summation goes over the bound states only and I stands for the incomplete Fermi-Dirac integral given by

$$I_{1/2}\left[\frac{u - V(r)}{kT}\right] = \int_{-V(r)/kT}^{\infty} t^{1/2}[\exp(t - \mu/kT) + 1]^{-1} dt . \tag{2.7}$$

For the exchange-correlation part of the potential we use a local potential given by Hedin and Lundqvist.[12] It should be noted that as a result of the Thomas-Fermi approximation of the free-electron density given by Eq. (2.7), such features as the well-known Friedel oscillations do not appear in our treatment.

So far everything that was stated is valid both for the IS-AA and IC-AA models. The difference between the two models appears via the boundary and normalization conditions. In the IS model, charge neutrality requires that

$$4\pi \int_0^{r_i} \rho_e(r) r^2 dr = Z , \tag{2.8}$$

where r_i is the ion-sphere radius given by

$$r_i = (3/4\pi N)^{1/3} \tag{2.9}$$

and N stands for the density of atoms in the plasma. Since the IS-AA atom is neutral within the ion sphere, the $V_+(r)$ term in the potential of Eq. (2.2) is absent. On the other hand, in the IC model, where the region of interest extends from zero to infinity, the charge neutrality requires that

$$4\pi \int_0^{\infty} [\rho_e(r) - \rho_+(r)] r^2 dr = Z . \tag{2.10}$$

The integral in Eq. (2.10) exists only if

$$\lim_{r\to\infty} \rho_e(r) = \lim \rho_+(r) = \rho_0 = Z^* N . \tag{2.11}$$

In Eqs. (2.10) and (2.11), $\rho_+(r)$ stands for the charge density of the positive ions and Z^* for the average effective charge (Z minus the bound electrons) of the ions.

At this point we have to discuss the computation of Z^*. In the IS model the problem is trivial; the summation term in Eq. (2.6) yields the number of bound electrons per ion, which also yields Z^*. In the IC model the number of bound electrons per ion is not obvious, because the weakly bound upper levels are shared between the central ion and the neighboring positive charges. We propose a simple way to account for the degree an electron is shared with the neighbors by calculating the integral

$$f_{nl} = \frac{1}{Z^*} \int_0^{\infty} R_{nl}^2(r) \rho_+(r) r^2 dr , \tag{2.12}$$

where R_{nl} stands for the radial part of the wave function Ψ_{nlm}. Therefore, in the IC model the number of bound electrons per ion is obtained if the occupancies are multiplied by the factors $1 - f_{nl}$. The same factor has to multiply the bound-bound and bound-free oscillator strengths for the calculation of photoabsorption per ions in the IC model. For the deeply bound levels, the $f_{nl}-s$ are practically zero, and for the upper levels in all of our study cases they never exceed a few percent.

In addition to the normalization conditions for the charges, the electronic wave functions are also subject to different boundary conditions in the IS and IC models. For the bound states in the IS model, the radial part of the one-electron wave function can have one of the two boundary conditions set at r_i:

$$R'_{nl}(r_i) = 0 \tag{2.13a}$$

or

$$R_{nl}(r_i) = 0 . \tag{2.13b}$$

At a finite r_i the boundary conditions (2.13a) and (2.13b) yield two different eigenvalues for ε_{nl}, which in an approximative way can be regarded as the lower and upper limits of an electronic band. If r_i is at infinity, the boundary conditions set by Eqs. (2.13a) and (2.13b) are satisfied simultaneously, predicting a discrete level, just like in the case of an isolated atom. The boundary conditions for the continuum states are discussed extensively in Ref. 11. Next we concentrate on the computation of $\rho_+(r)$ and $V_+(r)$ in the IC model.

We write $\rho_+(r)$ in the form

$$\rho_+(r) = \rho_0 g(r) , \tag{2.14}$$

where $g(r)$ has to satisfy the hypernetted-chain (HNC) integral equation[13]

$$\ln g(\mathbf{r}) + \beta V_I(\mathbf{r}) = N \int [g(\mathbf{r} - \mathbf{r}_1) - 1] \times [g(\mathbf{r}_1) - 1 - \ln g(\mathbf{r}_1) - \beta V_I(\mathbf{r}_1)] d^3\mathbf{r}_1 \tag{2.15}$$

and $V_I(r)$ is the effective ion-ion potential given by

$$V_I(r)=[Z^*(r)]^2/r \tag{2.16}$$

and b stands for $1/kT$. In Eq. (2.16), $Z^*(r)$ is a position dependent effective charge that takes into account the screening by the bound and free electrons. For $Z^*(r)$ we use the formula

$$Z^*(r)=Z-r[V_e(r)+V_+(r)] \ . \tag{2.17}$$

It is straightforward to show that Eqs. (2.16) and (2.17) account properly for the interaction between the nuclei and between a nucleus and the positive and negative charge clouds of a neighbor nucleus. With regard to the interaction between the extended clouds at intermediate separation, Eqs. (2.16) and (2.17) are not exact, but they give the correct limits at large and close separation. Therefore, we assume that the ion-ion interaction given by Eqs. (2.16) and (2.17) is adequate. We can also see from Eq. (2.15) that in the low density limit when $N\rightarrow 0$, $g(r)\rightarrow\exp[-\beta V_I(r)]$, which is the Debye-Huckel limit. Writing

$$\ln g(r)+\beta V_I(r)=y(r) \ , \tag{2.18}$$

Eq. (2.15) can be written as

$$y(\mathbf{r})=N\int[g(\mathbf{r}-\mathbf{r}_1)-1][g(\mathbf{r}_1)-1-y(\mathbf{r}_1)]d^3\mathbf{r}_1 \ . \tag{2.19}$$

The potential resulting from the ion distribution has to satisfy Poisson's equation,

$$\nabla^2 V_+(r)=4\pi\rho_+(r) \ . \tag{2.20}$$

Equation (2.19) for the ion-ion correlation is a one-component equation in the sense that we do not have a set of coupled equations for the ion-ion, electron-ion, and electron-electron correlation functions arising from many-body effects, so our model should be regarded as a one-particle model for the interacting electron-ion system. A more thorough treatment of the particle correlations is given by Chihara[14] and by Perrot *et al.*[15] For the present we believe that the main differences between the IC and IS models are sufficiently accounted for by the set of equations (2.1)–(2.20), which completely define the self-consistent AA state for the IS or IC model, whichever is applicable.

At this point we wish to emphasize that for the computation of photoabsorption the AA approximation is not sufficient. In order to obtain a realistic photoabsorption cross section in a plasma, it is necessary to go beyond the AA approximation and account for all the electronic states in a detailed fashion, which includes all the relevant many-electron configurations of the differently ionized specimen. In this paper, we calculate the spectra of the many-electron configurations of the differently ionized specimen in first-order perturbation using the self-consistent AA wave functions. We also use the AA wave functions for the computation of the bound-bound and bound-free dipole transition integrals. It should be noted that although we do not use the continuum wave functions for the free-electron density in the set of self-consistent equations, we do compute the latter for the bound-free transitions. The reason for the above discrepancy is due to the fact that a complete accounting of the free-electron density sometimes requires many hundreds of partial waves, which is not the case for the computation of the bound-free transitions. The electronic potential of each detailed quantum state reflects the basic features of the IS or IC models via the interaction of the bound electron configuration with the free electrons and positive charges. In accordance with the LTE assumption, we calculate the photoabsorption of each ionic specimen assuming that the probabilities of the ionic states are given by the Boltzmann statistics. A detailed description of this algorithm is given in a paper by Goldberg, Rozsnyai, and Thompson.[16] The emphasis in this paper is on the difference between the self-consistent AA-IS and AA-IC models upon which the more detailed photoabsorption calculations rest.

III. COMPUTATIONS

We present four study cases: (i) iron at $kT=125$ eV and at 4.46 g/cm^3 density; (ii) aluminum at $kT=100$ eV and at 4.5×10^{-3} g/cm^3; (iii) bromine at $kT=270$ eV and at 2.6×10^{-2} g/cm^3; (iv) a solar mixture of 14 elements at $kT=86.17$ eV at 2.82×10^{-2} g/cm^3. Photoionization cross sections for case (i) were reported in Ref. 9. For case (ii), which typically occurs in laser-produced plasmas, bremsstrahlung studies were reported in Ref. 11 and emissivity studies were published by Lamoureux, Moller, and Jaegle.[17] For case (iii), experimental measurements were reported by Bailey *et al.*[18] and theoretical calculations based on the IS model were published in Ref. 16. Case (iv) is of astrophysical interest, and it corresponds to the first point of the data base of solar opacities in a paper by Bahcall and Ulrich.[19]

The essential results of the calculations are shown in Table I. For the single Z plasmas we show Z^* for the self-consistent AA state together with the Fermi level.

TABLE I. Summary of computational results. κ_R stands for the Rosseland mean opacity.

				IS			IC	
Z	ρ (g/cm^3)	kT (eV)	Z^*	μ (eV)	κ_R (cm^2/g)	Z^*	μ (eV)	κ_R (cm^2/g)
26	4.46	125	11.65	-3.60×10^2	3.87×10^3	9.91	-3.58×10^2	4.40×10^3
13	4.50×10^{-3}	100	10.76	-8.66×10^2	8.43×10^1	10.63	-8.69×10^2	1.31×10^2
35	2.60×10^{-2}	270	25.48	-2.39×10^3	4.71×10^1	25.88	-2.92×10^3	4.23×10^1
SO1 MIX	2.82×10^{-2}	86.2		-5.03×10^2	4.79×10^1		-5.07×10^2	5.46×10^1

Table I also shows the Rosseland mean opacity for the statistical average of all the relevant electronic configurations. The compositions of the solar mixture is shown in Table II. More details are shown in the figures.

TABLE II. Composition of solar mixture.

Z	Mole fraction	Mass fraction
1	9.1911×10^{-1}	7.3003×10^{-1}
2	7.9425×10^{-2}	2.5051×10^{-1}
6	4.3401×10^{-4}	4.1078×10^{-3}
7	8.6590×10^{-5}	9.5572×10^{-4}
8	7.2029×10^{-4}	9.0810×10^{-3}
10	8.8610×10^{-5}	1.4093×10^{-3}
12	3.5570×10^{-5}	6.8144×10^{-4}
13	2.6200×10^{-6}	5.5705×10^{-5}
14	3.1450×10^{-5}	6.9604×10^{-4}
16	1.4630×10^{-5}	3.6965×10^{-4}
18	3.6400×10^{-6}	1.1458×10^{-4}
20	2.1200×10^{-6}	6.6956×10^{-5}
24	6.6000×10^{-7}	2.7042×10^{-5}
26	4.3050×10^{-5}	1.8945×10^{-3}

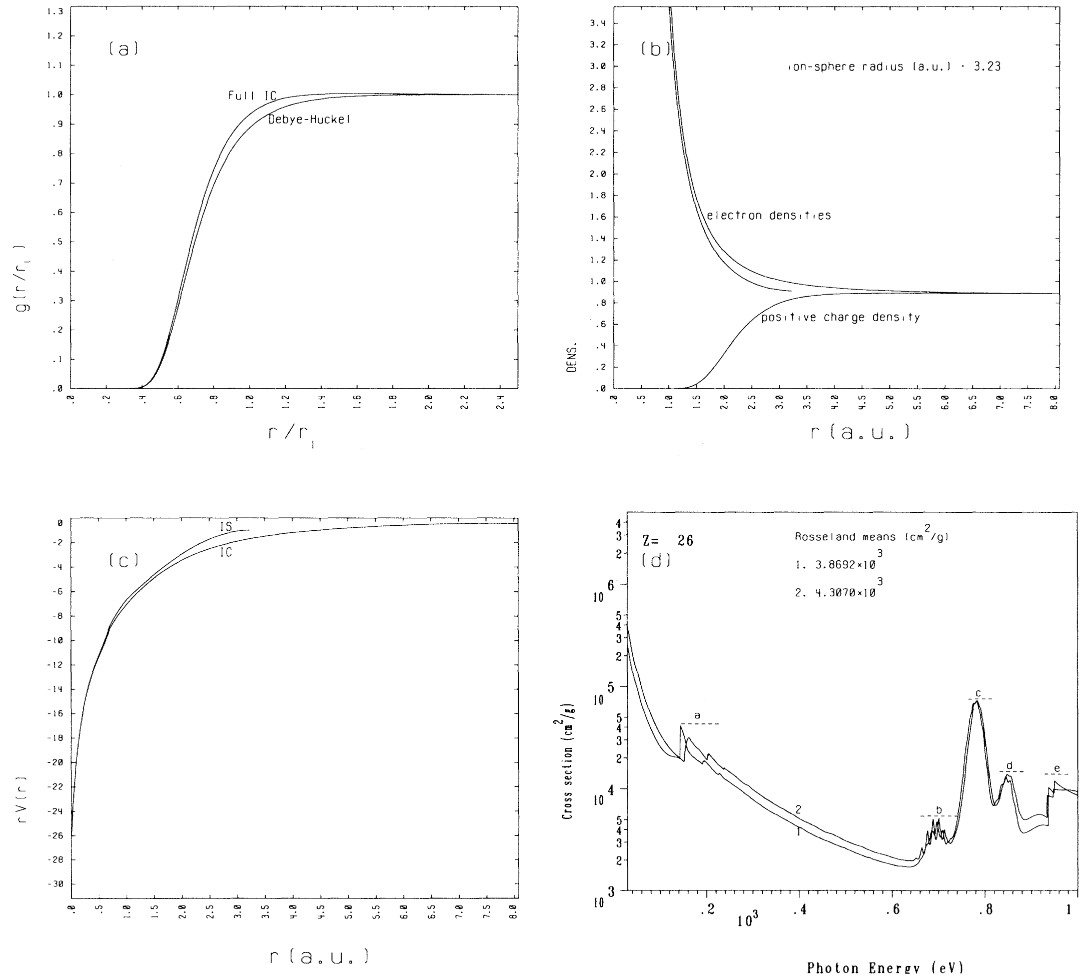

FIG. 1. Iron plasma at $kT=125$ eV and at 4.46 g/cm^3. (a) The ion-ion correlation function $g(r/r_i)$; (b) electron and positive charge densities; (c) self-consistent electron potential of the AA state multiplied by r; (d) total photoabsorption cross sections based on the IS (1) and IC (2) models. The symbols r and r_i stand for the distance from the central nucleus and for the ion-sphere radius, respectively. In (b) the electron density given by the IS model ends at the ion-sphere radius. In (d) the labels a, b, c, d, and e indicate the regions of the M-shell photoionization, the $2p$-$3s$, $2p_{3/2}$-$3d_{5/2}$-$2p_{1/2}$-$3d_{3/2}$ transition arrays, and the L-shell photoionization, respectively.

Figures 1 and 2 summarize the calculations for the iron and aluminum plasmas. In Figs. 1(a) and 2(a) we show the ion-ion correlation function arising from the solution of Eq. (2.19) and also in the Debye-Huckel limit. Figures 1(b) and 2(b) chow the charge densities of the AA state of the IS and IC models, Figs. 1(c) and 2(c) show the quantity $rV(r)$, where $V(r)$ is the electron potential of the AA state given by Eq. (2.2), and Figs. 1(d) and 2(d) show the total photoabsorption cross section predicted by the two models. Figures 1(d) and 2(d) also give the Rosseland mean opacities. The photoabsorption cross sections were computed after all the relevant ionic states of appreciable probability were calculated in first-order perturbation using the self-consistent AA wave functions. Actually, for the iron there were 85 electronic configurations distributed over the M and N shells from Na-like to Cl-like ions, and for the aluminum there were 15 electronic configurations distributed from Li- to N-like ions. Figures 1(d) and 2(d) show that the IC model predicts larger cross sections and Rosseland mean opacities than the IS model. The reason for this is due to the longer-range potential predicted by the IC model, in which there are slightly more bound electrons. The bound-free cross sections of the bound electrons provide a higher background for the line absorption. In addition, the free-free absorption or inverse bremmstrahlung is also stronger in the potential predicted by the IC model. The above constitutes the most important differences between the photoabsorption predicted by the two models and it is the essential point of this paper. It should be noted that in all the study cases presented here the ion-ion correlation function $g(r)$ does not show any oscillations. The reason for this is due partly to the relatively low values of the plasma coupling parameter and partly to the usage of the variable charge $Z^*(r)$ given by Eq. (2.17).

Figure 3 shows some physical details for the iron and aluminum plasmas. Figures 3(a) and 3(b) show the nearest-neighbor distribution function for the IC model given by [20]

$$W(r)=\frac{3}{r_i^3}g(r)r^2\exp\left[-\frac{3}{r_i^3}\int_0^r g(x)x^2dx\right] \tag{3.1}$$

and Figs. 3(c) and 3(d) show the microfield distribution given by[21]

$$H(\alpha)=\frac{2}{\pi}\alpha\int_0^\infty x\sin\alpha x\exp[-x^{(3+q)/2}/(\sqrt{x}+\Gamma)^q]dx\ , \tag{3.2}$$

where q is a constant, 1.2876.

The microfield distribution is important from the point of view of the Stark profiles of the spectral lines, thus it has an effect on the computed photoabsorption cross sections.

In Eq. (3.2) α is the reduced field strength E/E_0, where E and E_0 are the field strengths and normal field

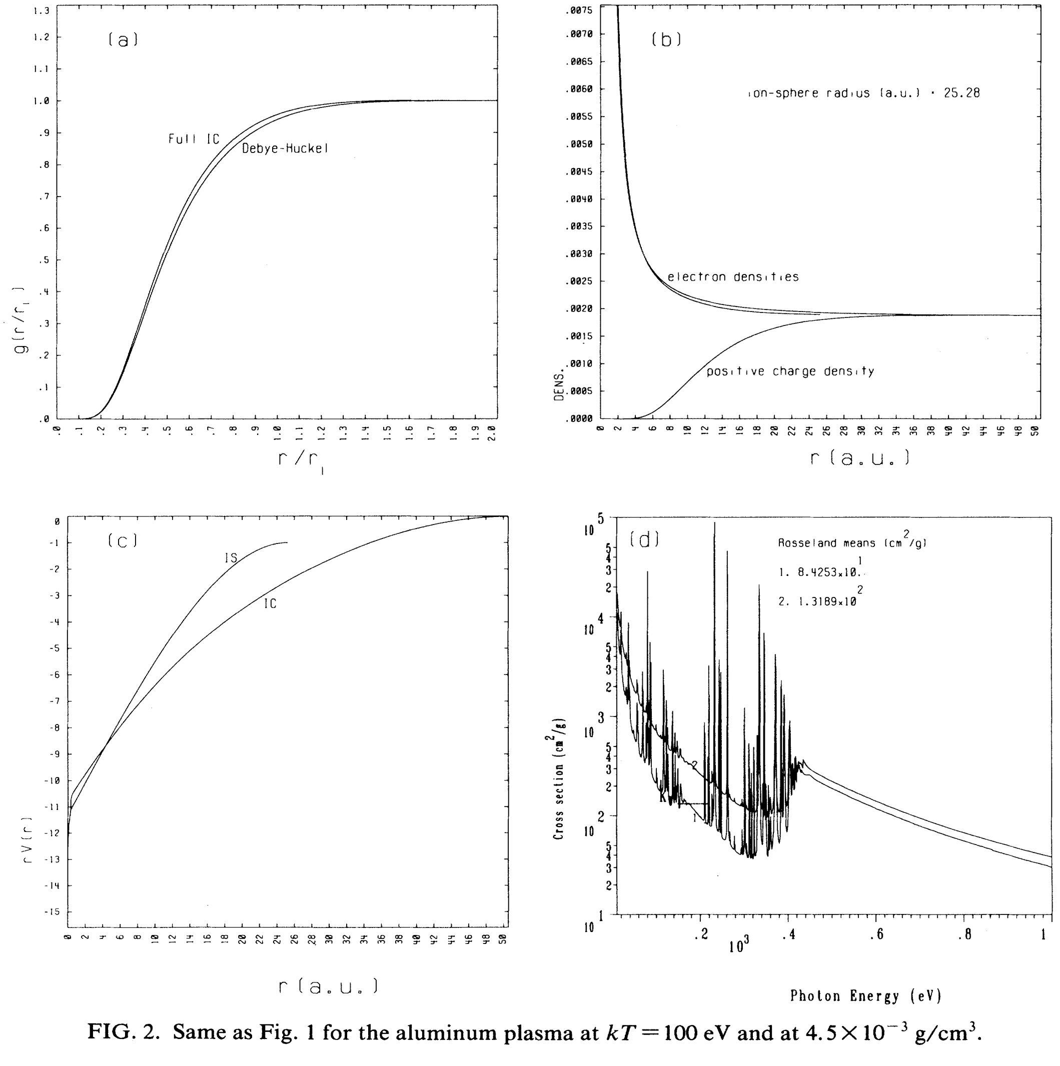

FIG. 2. Same as Fig. 1 for the aluminum plasma at $kT=100$ eV and at 4.5×10^{-3} g/cm^3.

strengths, respectively, and Γ is the plasma coupling parameter. The normal field strength E_0 and Γ is given by

$$E_0^i = Z^+/r_i^2 ; \Gamma = (Z^+)^2/kTr_i^2 \; . \qquad (3.3)$$

In Eq. (3.3), Z^+ is to be distinguished from Z^* to the extent that in the former the nuclear charge is reduced not only by the number of bound electrons, but also by the number of free electrons that are in the nonuniform cusp region of the free-electron density. Equation (3.2), which becomes a standard Holtsmark distribution when $\Gamma = 0$, assumes pointlike Coulomb interaction between the ions, so it is not consistent with the ion-ion correlation function $g(r)$. A precise computation of the microfield distribution consistent with all the charge distributions is outside of the scope of this paper, but due to the fact that the nearest-neighbor distribution peaks in the vicinity of the ion sphere, the author feels that Eq. (3.2) is acceptable for the microfield distribution.

The calculations for the bromine plasma are shown in Fig. 4. Figure 4(a) shows the experimentally measured emission intensity published in Ref. 18; Figs. 4(b) and 4(c) show the calculated emission intensity which is obtained from a simple solution of the radiative-transfer equation

$$I(\nu) = B(\nu)\{1 - \exp[\sigma(\nu)\rho L]\} \; . \qquad (3.4)$$

In Eq. (3.4), $I(\nu)$ is the intensity of the emerging radiation, $B(\nu)$ is the Planck function, $\sigma(\nu)$ the frequency-dependent photoabsorption cross section, ρ is the matter density and L is the average distance inside of the plasma through which the photons must pass before emerging and reaching the detector. For the sample thickness L, the value 2.4×10^{-3} cm was chosen corresponding to experimental conditions. Figure 4(d) shows the frequency-dependent cross section $\sigma(\nu)$ predicted by the IC model. We do not show the cross section predicted by the IS model because it is not visibly distinguishable from that of the IC model, although the predicted Rosseland mean opacities are different, as is evident from Table I.

Figure 5 shows the calculations for the solar mixture. Figure 5(a) shows the distribution function $g(r/r_i)$ as predicted by the IC model for the hydrogen and iron component of the mixture. In the case of the solar mix-

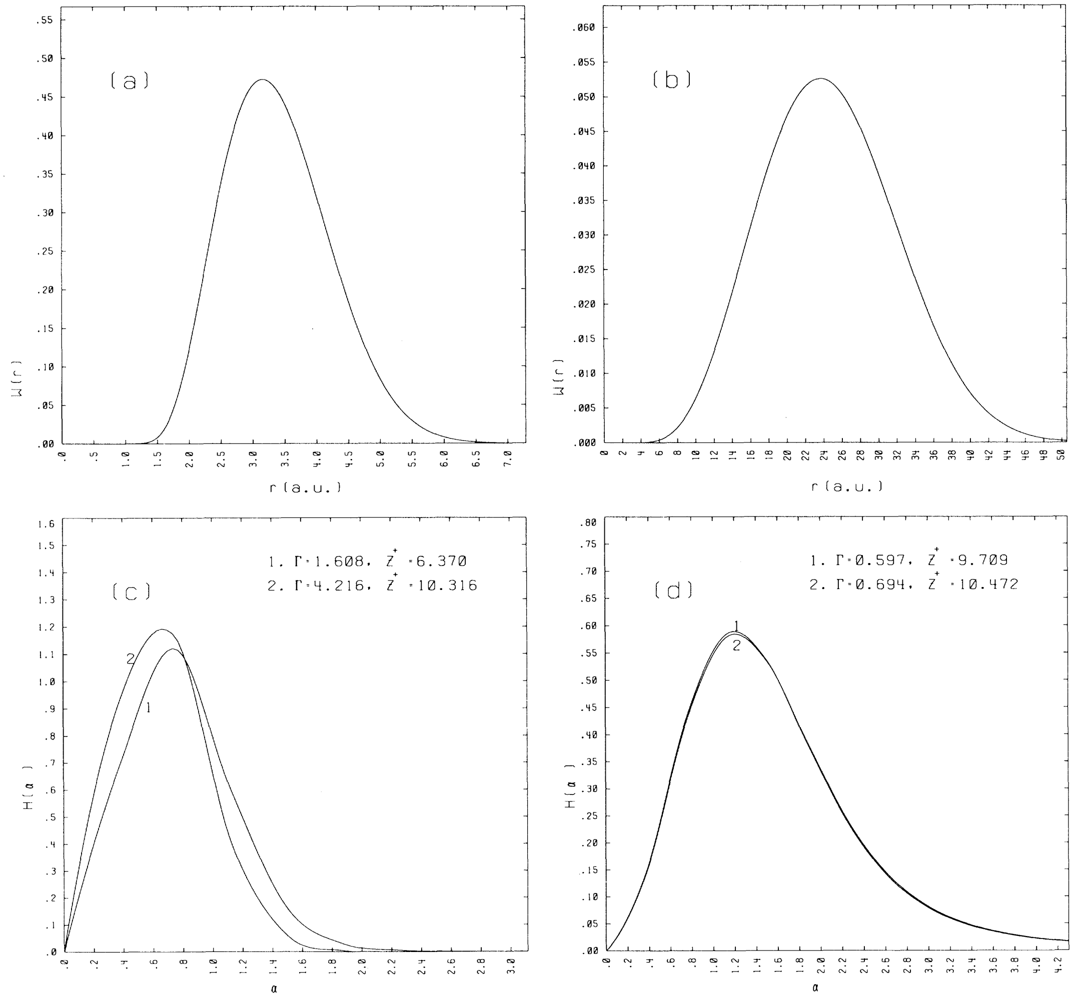

FIG. 3. Nearest-neighbor distribution predicted by the IC model, (a) and (b), and microfield distribution (c) and (d) for the iron and aluminum plasmas. Curve 1, IC model; curve 2, IS model.

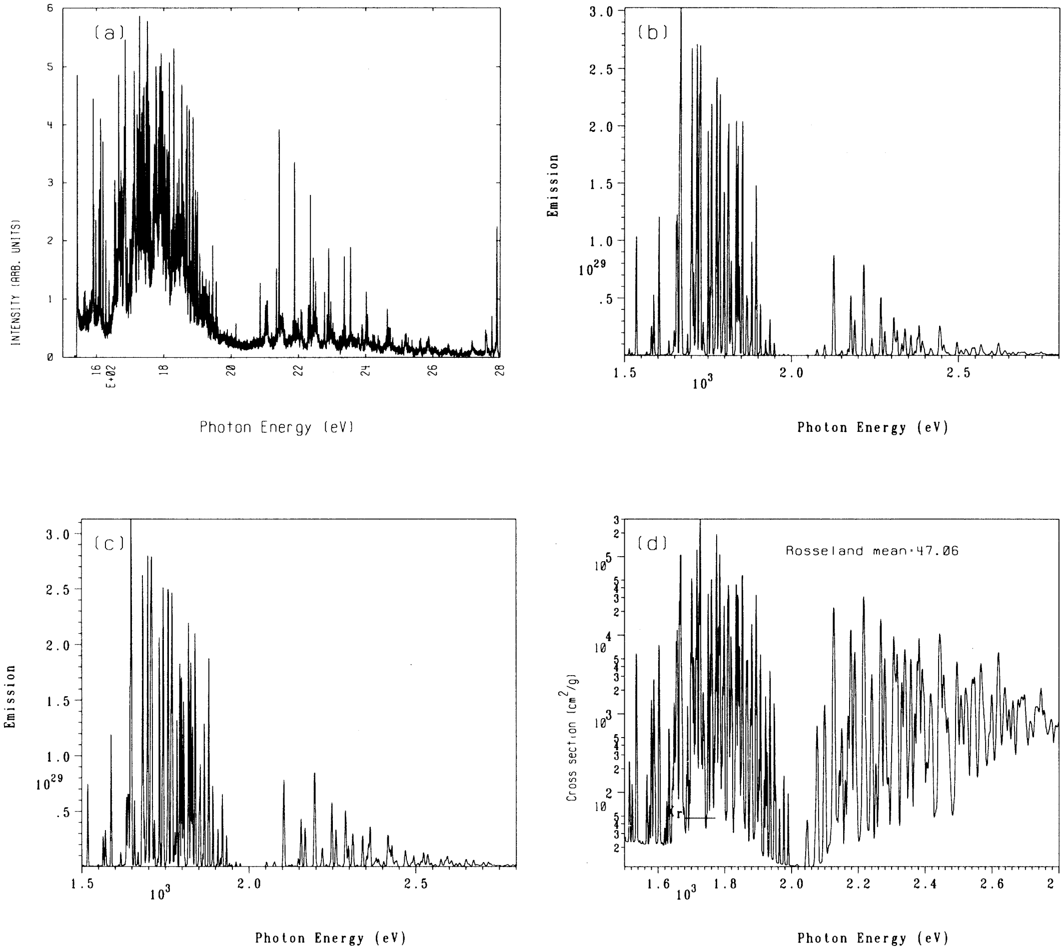

FIG. 4. Experimental data and calculations for bromine plasma at $kT=270$ eV and at 2.6×10^{-2} g/cm^3. (a) Measured emission spectra; (b) and (c), calculated emission predicted by the IS and IC models, respectively, with the usage of Eq. (3.4) and a thickness of 2.5×10^{-3} cm for the plasma; (d) total absorption cross section predicted by the IC model.

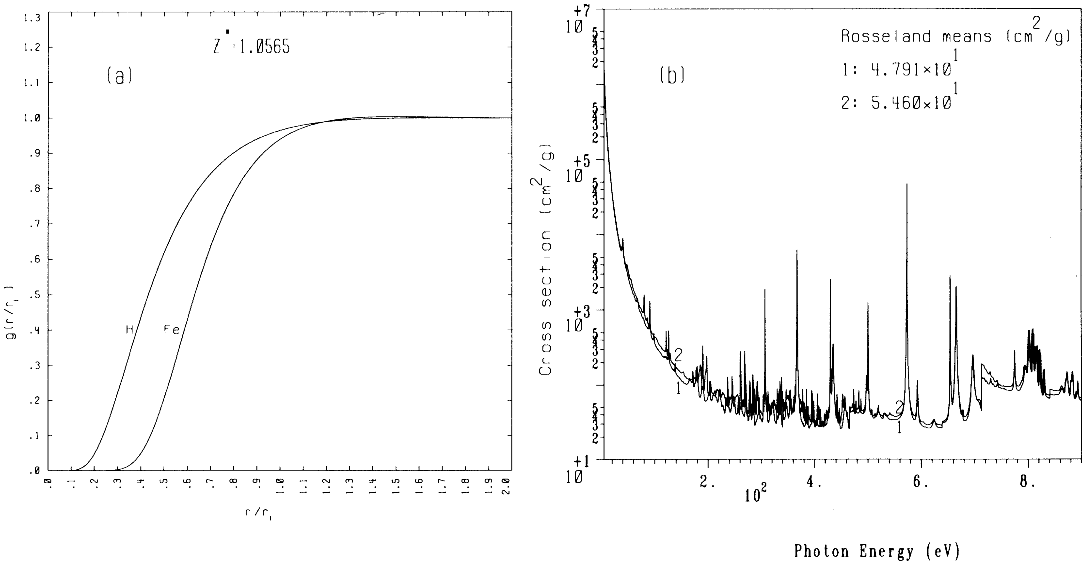

FIG. 5. Solar mixture at $kT=86.17$ eV and at 2.82×10^{-2} g/cm^3. (a) The function $g(r/r_i)$ for the hydrogen and iron component; (b) photoabsorption of the mixture predicted by the IS (1) and IC (2) models, respectively. Table I is on another document.

ture, $g(r)$ is the distribution function between the central ion of a component and the average perturber in the plasma, whose charge is calculated form the ionization state of each component and mole fractions given in Table II. For the other Z elements of the mixture, g is in between the hydrogen and iron curves. Figure 5(b) shows an overlay of the IC and IS photoabsorption cross sections. Most of the lines are contributed by the iron component with some contributions coming from argon calcium and chromium. As is evident, there is hardly a visible difference between the two curves, yet the difference in the Rosseland mean opacities is about 11%. In view of recent needs for accurate solar opacities, this difference is not negligible.

IV. DISCUSSION

The main purpose of this paper was to show the differences in the theoretically predicted photoabsorption of hot plasma arising not from computational approximations but from the fundamental differences in the theoretical models. In all the study cases the positions and strengths of the spectral lines are nearly indistinguishable between the IC and IS models, yet in some cases the difference between the predicted Rosseland mean opacities is significant due to the difference in the continuous bound-free and free-free absorption, which in turn is due to the fact that the IC model predicts a longer-range potential than the IS model. The author believes that this fundamental difference remains, even if the two models are subjected to more scrutiny. Obviously, as far as nature is concerned, neither of the two models presented in this parer may be correct, hopefully reality lies somewhere in between. Experimental verification of one model versus the other would be very difficult, because of the proximity of the spectral lines predicted by the two models. Here is a typical case where computer experiments could be very helpful. For example, the extension of the molecular-dynamics code of Car and Parrinello[22] to include photoabsorption could be very revealing. The author is not aware of such programs.

ACKNOWLEDGMENTS

Part of this research was done during the author's visit at the Institute for Theoretical Physics, University of California, Santa Barbara, at a workshop titled "Atoms and Ions in Plasmas." The author is grateful to the organizers of the workshop and to the Director of the Institute for giving an opportunity to work in a stimulating atmosphere. Work performed under the auspices of the U. S. Department of Energy by the Lawrence Livermore National Laboratory under Contract No. W-7405-ENG-48.

---

[1] A. S. Eddington, *The Internal Constitution of Stars* (Cambridge University Press, Cambridge, 1926).

[2] T. R. Carson, D. F. Mayers, and D. W. Stibbs, Mon. Not. R. Astron. Soc. **140**, 483 (1968).

[3] R. P. Feynman, N. Metropolis, and E. Teller, Phys. Rev. **75**, 1561 (1949).

[4] R. D. Cowan and J. Ashkin, Phys. Rev. **105**, 144 (1957).

[5] J. W. Zink, Phys. Rev. **176**, 279 (1968).

[6] B. F. Rozsnyai, Phys. Rev. A **5**, 1137 (1972).

[7] M. W. C. Dharma-wardana and F. Perrot, Phys. Rev. A **26**, 2096 (1982).

[8] F. Perrot and M. W. C. Dharma-wardana, Phys. Rev. A **29**, 1378 (1984).

[9] F. Perrot and M. W. C. Dharma-wardana, Phys. Rev. A **31**, 970 (1985).

[10] F. Grimaldi, A Grimaldi-Lecourt, and M. W. C. Dharma-wardana, Phys. Rev. A **32**, 1063 (1985).

[11] B. F. Rozsnyai and M. Lamoureux, J. Quantum Spectrosc. Radiat. Trans. **43**, 381 (1990).

[12] L. Hedin and B. Lundqvist, J. Phys. C **4**, 2064 (1971).

[13] J. P. Hansen and I. R. McDonald, *Theory of Simple Liquids* (Academic, New York, 1986), p. 119.

[14] J. Chihara, Phys. Rev. A **33**, 2575 (1986).

[15] F. Perrot, Y. Furutani, and M. W. C. Dharma-wardana, Phys. Rev. A **41**, 1096 (1990).

[16] A. Goldberg, B. F. Rozsnyai, and P. Thompson, Phys. Rev. A **34**, 421 (1986).

[17] M. Lamoureux, C. Moller, and P. Jaegle, Phys. Rev. A **30**, 429 (1984).

[18] J. Bailey, R. E. Stewart, J. D. Kilkenney, R. S. Walling, T. Phillips, R. J. Fortner, and R. W. Lee, J. Phys. B **19**, 2639 (1986).

[19] J. N. Bahcall and R. K. Ulrich, Rev. Mod. Phys. **60**, 297 (1988).

[20] See. S. Chanrashekhar, Rev. Mod. Phys. **15**, 1 (1943).

[21] B. F. Rozsnyai and T. Einwohner, in *Spectral Line Shapes,* edited by K. Burnett (de Gruyter, Berlin, 1983), p. 315.

[22] R. Car and M. Parrinello, Phys. Rev. Lett. **55**, 2471 (1985).